

The effects of growth rate and biomechanical loading on bone laminarity within the emu skeleton (#27991)

1

First revision

Guidance from your Editor

Please submit by **16 May 2019** for the benefit of the authors (and your \$200 publishing discount).



Structure and Criteria

Please read the 'Structure and Criteria' page for general guidance.



Custom checks

Make sure you include the custom checks shown below, in your review.



Author notes

Have you read the author notes on the [guidance page](#)?



Raw data check

Review the raw data. Download from the [materials page](#).



Image check

Check that figures and images have not been inappropriately manipulated.

Privacy reminder: If uploading an annotated PDF, remove identifiable information to remain anonymous.

Files

Download and review all files from the [materials page](#).

1 Tracked changes manuscript(s)

1 Rebuttal letter(s)

9 Figure file(s)

7 Table file(s)

! Custom checks

Vertebrate animal usage checks



Have you checked the authors [ethical approval statement](#)?



Were the experiments necessary and ethical?



Have you checked our [animal research policies](#)?




Structure and Criteria

Structure your review

The review form is divided into 5 sections. Please consider these when composing your review:

1. BASIC REPORTING
2. EXPERIMENTAL DESIGN
3. VALIDITY OF THE FINDINGS
4. General comments
5. Confidential notes to the editor






 You can also annotate this PDF and upload it as part of your review

When ready [submit online](#).





Editorial Criteria

Use these criteria points to structure your review. The full detailed editorial criteria is on your [guidance page](#).





BASIC REPORTING

-  Clear, unambiguous, professional English language used throughout.
-  Intro & background to show context. Literature well referenced & relevant.
-  Structure conforms to [PeerJ standards](#), discipline norm, or improved for clarity.
-  Figures are relevant, high quality, well labelled & described.
-  Raw data supplied (see [PeerJ policy](#)).

EXPERIMENTAL DESIGN

-  Original primary research within [Scope of the journal](#).
-  Research question well defined, relevant & meaningful. It is stated how the research fills an identified knowledge gap.
-  Rigorous investigation performed to a high technical & ethical standard.
-  Methods described with sufficient detail & information to replicate.

VALIDITY OF THE FINDINGS

-  Impact and novelty not assessed. Negative/inconclusive results accepted. *Meaningful* replication encouraged where rationale & benefit to literature is clearly stated.
-  Data is robust, statistically sound, & controlled.
-  Speculation is welcome, but should be identified as such.
-  Conclusions are well stated, linked to original research question & limited to supporting results.

Standout reviewing tips

3



The best reviewers use these techniques

Tip

Support criticisms with evidence from the text or from other sources

Example

Smith et al (J of Methodology, 2005, V3, pp 123) have shown that the analysis you use in Lines 241-250 is not the most appropriate for this situation. Please explain why you used this method.

Give specific suggestions on how to improve the manuscript

Your introduction needs more detail. I suggest that you improve the description at lines 57- 86 to provide more justification for your study (specifically, you should expand upon the knowledge gap being filled).

Comment on language and grammar issues

The English language should be improved to ensure that an international audience can clearly understand your text. Some examples where the language could be improved include lines 23, 77, 121, 128 – the current phrasing makes comprehension difficult.

Organize by importance of the issues, and number your points

1. Your most important issue
2. The next most important item
3. ...
4. The least important points

Please provide constructive criticism, and avoid personal opinions

I thank you for providing the raw data, however your supplemental files need more descriptive metadata identifiers to be useful to future readers. Although your results are compelling, the data analysis should be improved in the following ways: AA, BB, CC

Comment on strengths (as well as weaknesses) of the manuscript

I commend the authors for their extensive data set, compiled over many years of detailed fieldwork. In addition, the manuscript is clearly written in professional, unambiguous language. If there is a weakness, it is in the statistical analysis (as I have noted above) which should be improved upon before Acceptance.

The effects of growth rate and biomechanical loading on bone laminarity within the emu skeleton

Amanda L Kuehn¹, Andrew H Lee², Russell P Main³, Erin LR Simons^{Corresp. 4}

¹ Arizona College of Osteopathic Medicine, Midwestern University, Glendale, AZ, United States

² Department of Anatomy, College of Graduate Studies, Arizona College of Osteopathic Medicine, College of Veterinary Medicine, Midwestern University, Glendale, AZ, United States

³ College of Veterinary Medicine, Purdue University, West Lafayette, IN, United States

⁴ Department of Anatomy, College of Graduate Studies, Arizona College of Osteopathic Medicine, Midwestern University, Glendale, AZ, United States

Corresponding Author: Erin LR Simons
Email address: esimon@midwestern.edu

The orientation of vascular canals in primary bone may reflect differences in growth rate and/or adaptation to biomechanical loads. Previous studies link specific canal orientations to bone growth rates, but results between different taxa are contradictory. Circumferential vascular canals (forming laminar bone) have been hypothesized to reflect either (or both) rapid growth rate or locomotion-induced torsional loading. Previous work on the hindlimb biomechanics in the emu shows that the femur and tibiotarsus experience large shear strains, likely resulting from torsional loads that increase through ontogeny. Here, we test how growth rate and biomechanical loading affect bone laminarity in wing and hindlimb elements from growing emu (2 - 60 wks). If laminar bone is an adaptation to torsion-induced shear strains, it should increase from juveniles to adults. Alternatively, if bone laminarity reflects rapid growth, as has been shown previously in emu, it should be abundant in fast-growing juveniles and decrease with age. Transverse mid-shaft histological sections from the limb bones (femur, tibiotarsus, humerus, ulna, and radius) were prepared and imaged. Growth rates were measured using fluorescent bone labels. Vascular canal orientation was quantified using laminarity index (proportion of circumferential canals). Principal components analysis was performed to convert highly correlated variables (i.e., mass, age, growth rate, and shear strain) into principal components. Multiple beta regression and model selection were performed to determine which principal components best explained laminarity. Growth rates were found to be highest in young individuals for all five skeletal elements. In the femur and tibiotarsus, the ontogenetic axis is a major explanatory factor. Elevated laminarity is strongly correlated with adult features such as large size, old age, and slow growth rate. This result is contrary to predictions made based on a previous study of emu but support results observed in some other avian species (penguin, chicken). In the femur and tibiotarsus, shear strain is a

minor explanatory factor and the association with laminarity is not significant in our dataset. Laminarity in the wing elements is variable and does not correlate with growth rate or other ontogenetic factors. Laminar bone may form in wing bones due to relaxed developmental canalization or may be a retained ancestral feature. In conclusion, ontogeny (including growth rate) is the dominant influence on vascular canal orientation in the hindlimb of the emu.

The effects of growth rate and biomechanical loading on bone laminarity within the emu skeleton

Amanda L. Kuehn¹, Andrew H. Lee², Russell P. Main³, Erin L. R. Simons⁴

¹Arizona College of Osteopathic Medicine, Midwestern University, Glendale, AZ, USA

²Department of Anatomy, College of Graduate Studies, Arizona College of Osteopathic Medicine, College of Veterinary Medicine, Midwestern University, Glendale, AZ, USA

³College of Veterinary Medicine, Purdue University, West Lafayette, IN, USA

⁴Department of Anatomy, College of Graduate Studies, Arizona College of Osteopathic Medicine, Midwestern University, Glendale, AZ, USA

Corresponding Author:

Erin Simons¹

Email address: esimon@midwestern.edu

24 ABSTRACT

25 The orientation of vascular canals in primary bone may reflect differences in growth rate
 26 and/or adaptation to biomechanical loads. Previous studies link specific canal orientations to
 27 bone growth rates, but results between different taxa are contradictory. Circumferential vascular
 28 canals (forming laminar bone) have been hypothesized to reflect either (or both) rapid growth
 29 rate or locomotion-induced torsional loading. Previous work on the hindlimb biomechanics in
 30 the emu shows that the femur and tibiotarsus experience large shear strains, likely resulting from
 31 torsional loads that increase through ontogeny. Here, we test how growth rate and biomechanical
 32 loading affect bone laminarity in wing and hindlimb elements from growing emu (2 - 60 wks). If
 33 laminar bone is an adaptation to torsion-induced shear strains, it should increase from juveniles
 34 to adults. Alternatively, if bone laminarity reflects rapid growth, as has been shown previously in
 35 emu, it should be abundant in fast-growing juveniles and decrease with age. Transverse mid-
 36 shaft histological sections from the limb bones (femur, tibiotarsus, humerus, ulna, and radius)
 37 were prepared and imaged. Growth rates were measured using fluorescent bone labels. Vascular
 38 canal orientation was quantified using laminarity index (proportion of circumferential canals).
 39 Principal components analysis was performed to convert highly correlated variables (i.e., mass,
 40 age, growth rate, and shear strain) into principal components. Multiple beta regression and model
 41 selection were performed to determine which principal components best explained laminarity.
 42 Growth rates were found to be highest in young individuals for all five skeletal elements. In the
 43 femur and tibiotarsus, the ontogenetic axis is a major explanatory factor. Elevated laminarity is
 44 strongly correlated with adult features such as large size, old age, and slow growth rate. This
 45 result is contrary to predictions made based on a previous study of emu but support results
 46 observed in some other avian species (penguin, chicken). In the femur and tibiotarsus, shear

strain is a minor explanatory factor and the association with laminarity is not significant in our dataset. Laminarity in the wing elements is variable and does not correlate with growth rate or other ontogenetic factors. Laminar bone may form in wing bones due to relaxed developmental canalization or may be a retained ancestral feature. In conclusion, ontogeny (including growth rate) is the dominant influence on vascular canal orientation in the hindlimb of the emu.

INTRODUCTION

Avian bone tissue is highly vascularized with a fibrolamellar structure, which allows for rapid growth by depositing randomly arranged spicules of woven bone initially, followed by infilling of the cancellous spaces with centripetal lamellar bone, forming primary osteons (Francillon-Vieillot et al., 1990; de Ricqlès et al., 1991; Curry, 2002). Each primary osteon contains a central canal that houses blood vessels and nerves. These vascular canals vary in orientation and bones can be classified based on the predominant canal orientation. Laminar bone typically has a higher proportion of canals with circumferential orientation (parallel to the periosteal surface of the bone) relative to other orientations. Additional canal orientations include: radial, those orthogonal to the periosteal surface; longitudinal, those running parallel to the long axis of the bone; and oblique, all other orientations (de Ricqlès et al., 1991).

It has been hypothesized that differences in primary vascular canal orientation might be a reflection of growth rate, biomechanical loads, or phylogenetic relationships (Padian, 2013). Amprino (1947) first suggested that the organization of bone microstructure may be influenced by bone growth rate, such that woven bone is deposited during rapid growth and lamellar bone during slow growth (de Ricqlès et al., 1991). Further studies have investigated whether specific primary vascular canal orientations in fibrolamellar bone are also associated with slow or fast

growth by directly comparing microstructure with bone growth rates measured through the use of injectable fluorochromes (Castanet et al., 2000; de Margerie et al., 2002; de Margerie et al., 2004). Rapidly growing hindlimb bones of ratites have been found to exhibit structure that is laminar and reticular (bone with numerous obliquely-oriented canals), whereas the much slower growing wing elements of ratites exhibit reticular and longitudinal canal structure (Castanet et al., 2000). This suggests that laminar bone, in part, may reflect faster growth rates. This result was supported in a recent study of pigeon wing elements, which showed that peak laminarity (proportion of laminar bone) coincides with the growth spurt in each element (Ourfalian, Ezell & Lee, 2016). However, work on mallard long bones showed no relationship between growth rate and predominant vascular canal orientation (de Margerie et al., 2002). Additionally, in the king penguin, radially-oriented canals dominated in the fastest growing sections, not circumferential canals (laminar bone) (de Margerie et al., 2004). Likewise, chickens selected for fast growth showed limb bones with predominantly radial canals (Williams et al., 2004; Pratt and Cooper, 2018).

Laminar bone has been hypothesized to better resist torsional loading. In laminar bone, the bone tissue is arranged in ‘sheets’ or ‘plates’ between layers of circumferential canals. Shear strain is thought to flow continuously within these ‘sheets’, and thus the concentrated stresses on the bone tissue surrounding the canals is reduced (de Margerie et al., 2004). Indeed, bone elements that are hypothesized to predominantly experience torsional loads have been found to exhibit laminar bone. Laminar bone is found to be most abundant in the humerus, ulna, and femur in a large sample of flighted bird species (de Margerie, 2002; de Margerie et al., 2005). *In vivo* strain gauge studies have shown that these elements experience predominantly torsional loads in at least some species: the humerus in the pigeon during flapping flight, the ulna in the

93 turkey during wing flapping while on the ground, and the femur in the chicken and emu during
94 terrestrial running, (Rubin and Lanyon, 1985; Biewener and Dial, 1995; Carrano and Biewener,
95 1999; Main and Biewener, 2007).

96 A limitation of previous studies of laminar bone is the indirect comparison of bone
97 histology in one species with bone growth rates and/or *in vivo* strain gauge measures taken from
98 different species. In this study, we present an analysis of laminar bone in a species in which bone
99 growth rate and *in vivo* bone strain data were directly measured. The emu (*Dromaius*
100 *novaehollandiae*, Order Struthioniformes, Family Dromaiidae) is a flightless bird endemic to
101 Australia, but widely farmed in the US. The individuals included in this study comprise a growth
102 series that were previously injected with fluorescent bone labels and surgically implanted with
103 gauges to measure *in vivo* locomotor strains in the femur and tibiotarsus (Main and Biewener,
104 2007). Shear strains, produced by torsional loads about the bones' long axes, were the
105 predominant type of strain in the two bones and increased from juveniles to adults (Main and
106 Biewener, 2007). Although bone strains were not measured in the wing elements of these
107 individuals, emus have extremely reduced wings that have no known function other than
108 occasionally being raised to aid thermoregulation (del Hoyo et al., 1992; Maxwell and Larsson,
109 2007). Presumably, shear strains are negligible in the wing elements.

110 Therefore, if laminarity is an adaptation to torsion-induced shear strains, we predict that
111 hindlimb bone laminarity will increase from juveniles to adults. Consistent with this hypothesis,
112 we expect negligible laminar bone in the vestigial wing elements from juveniles to adults.

113 Alternatively, if bone laminarity reflects rapid growth (as has been shown previously in emu), it
114 should be abundant in juveniles and decrease with age as growth slows in adults for all elements.

115 Incorporating growth rate measurements, direct biomechanical data, and direct histological

classification of laminarity makes this study a first of its kind that will be able to clarify the importance of growth and mechanics on vascular canal orientation in emu limbs.

MATERIALS & METHODS

This study samples forelimb and hindlimb elements from eight emus ranging in age from 2 to 60 weeks (Table 1). Birds used in this study were euthanized as part of a previous study (Main and Biewener, 2007) and the selected elements stored frozen. Emus were originally obtained as hatchlings by R.P. Main (at the time at Harvard University) from commercial farms (Songline Emu Farm, Gill, MA, USA; Scattered Oaks Emu Farm, Iola, TX, USA; Deep Hollow Farm, Oakdale, CT, USA) and raised at Harvard University's Concord Field Station (Bedford, MA, USA) under Harvard FAS IACUC approval AEP 23-15. For the first eight weeks of life the emus were held in large indoor enclosures, and then moved into pasture-sized outdoor enclosures. All birds had free access to commercial ratite diet (Mazuri, PMI Nutrition International, LLC, Brentwood, MO, USA) and water. Male and female birds were included based on availability. Emus exhibit a minor degree of sexual dimorphism, with females being slightly larger on average (del Hoyo et al., 1992). The difference in size is not large enough to be considered a confounding factor for this study.

As a part of a previous study (Main and Biewener, 2007), each bird was given a single intramuscular injection of xylenol orange (80mg/kg) followed by calcein (30mg/kg). Injections were given one week apart in birds less than 16 weeks of age and two weeks apart in birds between 16 and 65 weeks of age. Xylenol and calcein are fluorescent labels that are incorporated rapidly into newly mineralizing surfaces of bone at the time of injection (An and Martin, 2003). Thus, the time elapsed and the space between xylenol and calcein labels allows the calculation of

periosteal (radial) growth rate. One week after the last injection, surgery was performed to attach strain gauges to the cranial, caudal, and lateral aspects of the left femur and the cranial, caudal, and medial aspects of the left tibiotarsus. Single element strain gauges were used on the lateral femur and cranial and medial tibiotarsus. Rectangular rosette gauges were used on the cranial and caudal femur and caudal tibiotarsus. Rosette strain gauges allow both tensile and compressive principal strains and their orientations to be measured, and were placed so the central element of the gauge was parallel to the long axis of the bone. One day after surgery, the birds were run on a treadmill over a wide range of speeds and gaits. The raw data produced from the strain gauges were converted from voltage to microstrain using a custom MATLAB program. Shear strains were calculated from the rosette strain gauges using standard equations (Biewener and Dial, 1995). High quality shear strain data were most consistently collected from the caudal cortices of the femur and tibiotarsus and that is what is reported here. Trials in which the birds ran with a duty factor near 0.50 are included in the shear strain analysis (mean \pm SD: 0.50 \pm 0.02). Duty factor is the proportion of the time that the animal's foot spends on the ground during a stride relative to the entire stride time. A duty factor of 0.50 represents the point at which the birds transition to a running gait that incorporates an aerial phase. This is a relatively slow run for emu, but represents the duty factor for which we could maximize the number of animals included in this study based upon successful strain gauge function. Each trial was represented by five footfalls and, generally, two trials were collected for each bird. Following bone strain data collection, animals were euthanized. After death, whole wings were removed from the individuals and stored frozen. Histological sections of the femora and tibiotarsi were prepared (see Main and Biewener, 2007 for details) and shipped with the frozen wings to Midwestern University.

Histological Preparation

Emu wings were thawed and feathers, skin, muscles, and tendons were reflected to expose the skeletal elements. Both right and left wings were used based on availability. Using digital calipers, total length of each bone was measured and recorded. A 37-mm segment was removed using a Dremel tool from the mid-shaft region of the humerus, ulna, and radius. For two and four week old individuals whole elements were harvested due to their small size. Segments were labeled with permanent marker to maintain orientation. Dissected bone segments were placed in 10% neutral buffered formalin for fixation, then dehydrated in a graded ethanol series (70%, 85%, 100%) under vacuum. Segments were cleared with a xylene-substitute (Histo-clear; National Diagnostics, Atlanta, Georgia, USA). The bone segments were then vacuum- infiltrated and embedded in glass vials using Osteo-Bed Plus Resin, a two-part methyl methacrylate (Polysciences Inc.). Vials were placed in a 32° C bead bath to fully harden.

Once the resin hardened, vials were broken and two roughly 800-μm transverse sections were cut using a diamond blade saw (Isomet 1000; Buehler, Lake Bluff, Illinois, USA). These sections were attached to frosted glass slides using two-ton epoxy (Devcon, Milpitas, California, USA), keeping consistent spatial orientation. Slides were then ground to a thickness of 100±10μm using a graded scale of grit paper on a stand grinder (Metaserv 250; Buehler, Lake Bluff, Illinois, USA) and coverslipped with Permount (Fisher Scientific). The histological preparation was modified from An and Martin (2003) and closely followed Lee and Simons (2015).

Image Collection

The undecalcified sections contain xylenol (orange) and calcein (green) fluorochromes that were incorporated into newly mineralizing bone at the time of injection (see above for

injection schedule). These fluorochromes create stable long lasting tags (van Gaalen et al., 2010) and were examined under bright-field and fluorescent illumination with a motorized epifluorescent microscope (IX73, Olympus). The xylenol (orange) and calcein (green) tags were revealed using TRITC and FITC filter cubes, respectively, and a multichannel (red, green, bright-field) image of each section was generated with imaging software (cellSens, Olympus). Sufficient optical resolution (10X UPlanAPO $\approx 0.84 \mu\text{m}$; 20X UPlan S-APO $\approx 0.45 \mu\text{m}$) allowed a dual color-monochrome camera (DP80, Olympus) to capture high quality images (10X = $1.02 \mu\text{m}/\text{pixel}$; 20X = $0.51 \mu\text{m}/\text{pixel}$).

Calculating Bone Laminarity and Radial Growth Rates

Bright-field and fluorescent images were obtained from the wing and hindlimb elements (Figs. 1 and 2) and divided into equal octants from the estimated bone centroid. Four octants representing the cardinal anatomical positions (wing elements: cranial, caudal, dorsal, ventral; hindlimb elements: cranial, caudal, lateral, medial) were extracted (Fig. 2). Using ImageJ, each extracted octant was then uncurved using the “Straighten” function. The purpose of straightening was to standardize the periosteal tangent line so that appropriate measurements could be made in classifying the orientation of the vascular canals (Lee and Simons, 2015). To ensure there was minimal deformation of the image during the straightening process, known test angles were placed upon the image and measured in relation to the periosteal surface after the straightening function had been applied. Only those images with an average deformation less than or equal to 10° were accepted.

Within each of the four octants, the calcein green and xylenol orange tags were outlined with two reference lines. The distance between reference lines was measured at 10 equally spaced points in each octant. Growth rate was measured by taking the mean distance between

consecutive fluorescent tags divided by number of days between injections (Fig. 2C).

Degree of laminarity (Laminarity Index, LI) was measured in the interval of bone between the fluorochrome reference lines across all four octants. Using ImageJ, an ellipse was drawn within each in-focus primary vascular canal in the measurement interval (Fig. 2D). Branching canals were separated at branch points and counted individually. Multiple ellipses were drawn in curved canals. The aspect ratio and angle at which the ellipse sat in relation to the straightened periosteal surface was measured. We used the criteria set forth by de Margerie (2002) to classify the orientation of the vascular canals: (1) “circular” (circumferential) canals are oriented parallel ($0^\circ \pm 22.5^\circ$) to the periosteal surface of the bone; (2) radial canals are orthogonal ($90 \pm 22.5^\circ$) to the periosteal surface; (3) longitudinal canals run parallel to the long axis of the bone and have ellipses with an aspect ratio of less than 3; (4) oblique canals are all other orientations. Only primary vascular canals were measured. Secondary osteons in the sample area were excluded. We used a simple proportion (number of circumferential canals to the total number of canals) to estimate laminarity. To test the growth hypothesis, we used the laminarity index calculated from all sampled octants (Table 2, Table S1). Because consistent high quality shear strain data are only available from the caudal octant, we used the laminarity index calculated from only the caudal octant to test the mechanical hypothesis (Table 3, Table S2).

Principal Component Analysis (PCA) and Beta Regression

Because we sampled growing emus to test whether laminarity depends primarily on growth rate (growth hypothesis) or shear strain (mechanical hypothesis), mass and age become confounding variables. Mass and age covary with several biological variables including each other (Goonewardene et al., 2003), growth rate (Montes et al., 2005), and shear strain (Main &

231 Biewener, 2007). To minimize this multicollinearity, the variables of mass, age, growth rate and
 232 shear strain were normalized with log10-transformation and transformed to principal components
 233 (“princomp”: R Core Team, 2018). The proportion of total variance explained by each principal
 234 component (PC) and the eigenvectors of the variables that contribute to each PC are listed in
 235 Table 4.

236 The scores of the specimens along the PC axes and laminarity index (LI) were further
 237 examined using regression analysis. Because LI is a proportion between 0 and 1 and follows a
 238 beta distribution, linear regression is inappropriate. A standard procedure for making proportions
 239 interpretable with linear regression is arcsin transformation. However, such transformation can
 240 yield nonsensical predictions on the original scale and result in loss of statistical power (Warton
 241 and Hui, 2011). An alternative method to analyze proportions is to rescale the effective interval
 242 of the data to [0.005, 0.995] to avoid values of 0 and 1 (Smithson & Verkuilen, 2006) and apply
 243 beta regression (Ferrari & Cribari-Neto, 2004), which we implemented using the the betareg
 244 library (Cribari-Neto & Zeileis, 2010) in R (R Development Team, 2018). We performed three
 245 sets of beta regression: (1) forelimb elements; (2) hindlimb elements; and (3) caudal octant of
 246 hindlimb elements. Within each set, we evaluated several regression models of increasing
 247 complexity. The simplest models regressed laminarity (from all four octants or just the caudal
 248 value) on PC 1 or PC 2 in isolation as well as in additive combination. We also examined the
 249 effect of element type when treated as an additive factor (different intercepts but common slope)
 250 or multiplicative factor (different intercepts and slopes). To compare regression models (Table 5)
 251 and select the ones with the “best” fit to the data, we applied the small-sample correction of
 252 Akaike’s Information Criterion (AIC_c) (Hurvich & Tsai, 1989). In general, the best supported
 253 model has the lowest AIC_c value (Burnham & Anderson, 2002). Relative support between the

best and alternative models was assessed with difference (ΔAIC_c) values. Alternative models with ΔAIC_c values greater than 3, which is equivalent to a p -value of 0.051 (Taper, 2004), were rejected as having weak support.

RESULTS

Measured growth rates ranged from 1.33 $\mu\text{m}/\text{day}$ (radius of 48 week old individual) to 162.62 $\mu\text{m}/\text{day}$ (femur of 4.6 week old individual) (Table 2). Additive laminarity indices from all octants ranged from 0 to 0.58 (Table 2, Table S1, Fig 3). Laminarity indices from the caudal octant only ranged from 0 to 0.81 (Table 3, Table S2).


Summary of Caudal Octants from the Femur and Tibiotarsus

Table 4 shows that the first two principal components (PCs) account for 95% of the cumulative variance—75% by PC 1 (eigenvalue = 3.001) and 20% by PC 2 (eigenvalue = 0.812). Mass, age, and growth rate contribute strongly to PC 1, forming an “ontogenetic axis” with juvenile features at one end (small size, young age, and fast growth rate) and adult features at the other (large size, old age, and slow growth rate). Shear strain contributes somewhat to PC 1, but its residual variation dominates PC 2 to form a “shear strain axis” (Fig. 4).

In the best supported beta regression model (Table 5), the “ontogenetic axis” explains ~43% of the variation in the caudal octant laminarity. Higher laminarity values are correlated with adult features of ontogeny including large size, old age, and slow growth rate, whereas lower laminarity values are correlated with juvenile features ($p = 0.005$).

There is support for a model that predicts caudal octant laminarity based on the “ontogenetic axis” and the “shear strain axis” ($\Delta AIC_c = 1.4$; Table 5). This model explains ~61% of the total variation in caudal octant laminarity—the “ontogenetic axis” accounts for ~43%,

whereas the “shear strain axis” accounts for 18%. When the effect of shear strain is controlled, increasing ontogenetic features predict higher laminarity values ($p = 0.002$: Table 5; Fig. 5A).

 When the effect of ontogeny is controlled, there is a weak positive association between laminarity values and shear strain ($p = 0.052$: Table 5; Fig. 5B). Note that the two best models find strong support for a single relationship common to the femur and tibiotarsus; alternative models that treat element as an additive or multiplicative factor have essentially no support ($\Delta AIC_c \gg 4$: Table 4).

Summary of Cardinal Octants from the Femur and Tibiotarsus

Strain data are excluded from this analysis because it was not collected for all cardinal octants. Consequently, PC 1 (eigenvalue = 2.835), consisting of mass, age, and growth rate, accounts for 94% of the cumulative variance and forms an “ontogenetic axis” (Fig. 6). PC 2 (eigenvalue = 0.157) consists of the residual variation in (i.e., “ontogeny-independent”) growth rate and accounts for 5% of the cumulative variance (Table 4).

The best supported beta regression model predicts that ~70% of the variation in laminarity is explained by the “ontogenetic axis” (Table 5). Whereas juvenile features (e.g., small size, young age, and rapid growth rate) are correlated with lower laminarity values, adult features are correlated with higher laminarity values ($p < 0.001$). An alternative model ($\Delta AIC_c = 2.8$: Table 5) that treats element as an additive factor (i.e., elements have different regression intercepts but equivalent slopes) explains an additional 2% of the variation in laminarity (Fig. 7).

Summary of Cardinal Octants from the Humerus, Ulna, and Radius

In the absence of strain data for the forelimb elements, mass, age, and growth rate dominate PC 1 (eigenvalue = 2.614), and this “ontogenetic axis” accounts for 87% of the cumulative variance (Table 4, Fig. 8). An additional 12.6% of the variance is explained by

300 “ontogeny-independent growth rate” along PC 2 (eigenvalue = 0.377).

301 In the best supported model, 39% of the variation in laminarity is explained by
 302 “ontogeny-independent growth rate” (Table 5). This model predicts a positive correlation
 303 between both variables ($p = 0.0001$). An equally plausible model ($\Delta AIC_c = 1.6$: Table 5) adds
 304 “ontogenetic axis” as an additive covariate, which explains an additional 4–5% of the variation
 305 in laminarity. When the effect of “ontogenetic axis” is controlled, this alternative model predicts
 306 a significant positive correlation between laminarity and “ontogeny-independent growth rate” (p
 307 $= 8.77e-5$, Fig. 9B). However, when the effect of “ontogeny-independent growth rate” is
 308 controlled, a correlation between laminarity and “ontogenetic axis” is not significant ($p = 0.287$,
 309 Fig. 9A). Note that the two best models find strong support for a single relationship common to
 310 humerus, ulna, and radius; alternative models that treat element as an additive or multiplicative
 311 factor have essentially no support ($\Delta AIC_c \gg 4$: Table 4).


312

313 **DISCUSSION**


314 **Does bone laminarity reflect fast growth?**

315 The highest growth rate in all elements was found in the femur of the 4.6-week old
 316 individual (Table 2). As expected, hindlimb elements had higher growth rates than forelimb
 317 elements, reaching a maximum of 163 $\mu\text{m}/\text{day}$ in the femur and 99 $\mu\text{m}/\text{day}$ in the tibiotarsus.
 318 The humerus grew the fastest of the wing elements, reaching a maximum rate of 25 $\mu\text{m}/\text{day}$
 319 measured in the 2.3 and 4.6 week old individuals. Birds older than 8 weeks experienced a drastic
 320 decrease in bone growth rate in both hindlimb and forelimb elements. Previous analysis of emu
 321 somatic growth rate (increase in body mass) showed the maximum rate of growth (inflection
 322 point) to be about 15-17 weeks of age (Goonewardene et al., 2003). Our results suggest

maximum bone growth occurs much earlier (about 5 weeks) and is not an accurate proxy for the somatic growth inflection.

Principal components analysis reveals variance along an “ontogenetic axis” (Figs. 4, 6, 8). At one end of the axis, juvenile traits such as small size, young age, and rapid growth dominate. Adult traits such as large size, old age, and slow growth characterize the other end. This “ontogenetic axis” has a significant influence on laminarity in the femur and tibiotarsus ($p < 0.005$), whether analyzed in a single octant or cumulatively across several ones (Figs. 5A, 7). Elevated laminarity in the hindlimb appears correlated with adult size/age and  slow growth rate. This relationship is consistent with findings in the king penguin that also reported laminar bone to be associated with lower growth rates in four limb bones: femur, tibiotarsus, humerus, and radius (de Margerie et al., 2004). More recently, a study using microCT to assess three-dimensional vascular canal orientation in the humerus and femur of growth-controlled broiler chickens also found elevated laminarity in a slow-growing (feed-restricted) group (Pratt and Cooper, 2018). Interestingly, the effect of the “ontogenetic axis” on laminarity in the wing elements is weak ($p = 0.287$), only explaining 4–5% of variation (Fig. 9A). The weakened “ontogenetic axis” in wing bone laminarity is consistent with relaxed selection on the vestigial wing leading to increased anatomical variability in the species (Maxwell & Larsson, 2007). Residual variation in growth rate (“ontogeny-independent growth rate”) does explain a modest amount of variation (39%: Table 5) and is positively correlated with laminarity in the wing elements ($p = 2.73e-8$: Table 5, Fig. 9B). However “ontogeny-independent growth rate” is not relevant in the hindlimb elements, so it may be a mathematical artifact rather than a biological property.

Notably, our results differ from those previously reported for young emu bones in which

laminar and reticular bone was found in the fastest growing hindlimb bones (Castanet et al., 2000). In particular, Castanet et al. (2000) found laminar bone to be most abundant in the femur and tibiotarsus of emu less than 2 months of age, which corresponds to the youngest individuals in our study. Based on reported body masses, the emus included in our study were about 2-3 times heavier than the emus in the Castanet et al. (2000) study for a given age (Table 1). The reason for the differences in size and ontogenetic patterns for bone vascularity types between these two emu samples remain unknown, but could be related to genetic, dietary, or rearing conditions between the two groups. If laminarity is associated with lower growth rates, the youngest emus we studied may have been growing too fast for laminar bone to form. The greatest growth rate measured was in the femur of the 4.6-week-old bird (162.62 $\mu\text{m}/\text{day}$), which was about twice the fastest growth rate found in the femoral reticular bone tissue reported in the prior study (89.4 $\mu\text{m}/\text{day}$). Our study did not specifically address reticular bone, but by taking the proportion of oblique vascular canals (a “reticular index”), we found the amount of reticular bone in the fastest growing individual to be low in the hindlimb elements (femur and tibiotarsus: 0.17), and moderate to high in the wing elements (humerus: 0.62, ulna: 0.58, radius: 0.45). This result is, at least, consistent with the previous study because Castanet et al. (2000) found reticular bone to be more abundant in the humerus. The data analysis in the earlier emu study (Castanet et al., 2000) was conducted before a more rigorous method for quantifying canal orientation was developed (de Margerie, 2002), which may contribute to the observed differences between the two separate emu populations. Regardless, the results of the present study do not support the hypothesis that high laminarity reflects rapid growth in the emu and instead link higher laminarity with  slower growth rates.

Does bone laminarity reflect biomechanical load?

Within the caudal octants of the hindlimb elements, we found a non-significant positive association between laminarity and shear strain ($p = 0.052$; Table 5, Fig. 5B). Given the amount of variation (18%) explained by PC 2 (strain axis), we may conclude that torsion-induced shear strain has a small influence on the formation of laminar bone. Coincidentally, the mean laminarity across all ages of emu was generally (though not statistically) larger for the femur (0.41) than the tibiotarsus (0.28), which corresponds to the larger shear strains experienced in the femur (Main and Biewener, 2007). The shear strain magnitudes at the midshaft of the emu femur and tibiotarsus increased with age by only 2-3 times, whereas body mass increased by 46 times. Elevated laminar bone tissue, in combination with increased bone mineralization and decreased bone curvature during growth, may have helped mitigate shear strains despite the large increase in mass (Main and Biewener, 2007).

Although our results clearly show that ontogenetic factors largely influence the formation of laminar bone, torsional loading is a minor additional factor. However, the weak association between laminarity and shear strain limits the predictive potential of this relationship. Our results for emu hindlimb bones are consistent with previous studies of other torsionally-loaded limb elements. For example, when comparing wings of similar shape, laminarity in wing bones can be similar despite differences in presumed biomechanical load associated with unique primary flight modes (Simons and O'Connor, 2012; Marelli and Simons, 2014). In addition, preferred flight mode may only have subtle effects on overall loading of the bones, with the dominant loads being the high strains present during take-off (Biewener and Dial, 1995). Furthermore, there is also at least one example of a bone loaded predominantly in torsion that does not exhibit laminar bone, the bat humerus. The lack of laminarity in this (suspected) torsionally-loaded humerus is presumably due to the slow somatic growth rates of bats (Swartz, Bennet & Carrier, 1992; Lee

and Simons, 2015).

In this study, age groups are represented by one individual, with the exceptions of the youngest and oldest age groups that contain two. A larger sample of individuals in each age group would allow for investigation of how individual variation may or may not affect the relationship between LI, shear strain, and growth rate. Laminarity indices can be quite variable among individuals in some species. The pigeon humerus, which has been shown to experience large torsional loads, has been documented to exhibit both high and low laminarity in different individuals (Ourfalian et al., 2016; Lee and Simons, 2015; Skedros and Doutré, 2019). Similarly, a pooled sample of humeri from eight individual Red-tailed hawks show LI values that range from 0.30-0.70 (Simons and O'Connor, 2012; Marelli and Simons, 2014). Whether these variability patterns are biological or methodological is unclear. Laminarity measured on a histological section is a 2-dimensional representation of a 3-dimensional meshwork of vascular canals in cortical bone. This research is limited by the assumption that one or two closely placed mid-shaft histological sections are an accurate representation of vascular canal structure. MicroCT-based assessment of the three-dimensional network of vascular canals suggests that traditional 2D histological methods may overestimate LI, but also recognizes that these differences may be methodological (Pratt and Cooper, 2017; Pratt et al., 2018). Certainly, future studies should continue to use microCT to assess how well laminarity measured on histological sections represents actual biological structure. In addition, the torsional resistance in bones may more likely be linked to the specific orientation of another histological feature: collagen fibers. Collagen fiber orientation (CFO) has been shown to reflect principle strain distributions (Riggs et al., 1993; Skedros and Hunt, 2004; Skedros et al., 2004). Analysis of CFO is beyond the scope of the current study. However, given the known positive correlation between transversely

oriented collagen fibers and bone laminarity (de Margerie et al., 2005), we would expect a similar pattern for the femora and tibiotarsi examined here.

Although there is no direct biomechanical data for the forelimb elements of these birds, the wing elements presumably experience minimal loading. The emu wing is extremely reduced in size, even when compared to other ratites, and has almost no observed function (del Hoyo et al., 1992). Wing muscles of emu contain primarily slow acting tonic muscle fibers that may not allow much wing movement (Maxwell and Larsson, 2007), which suggests the underlying wing elements would experience minimal biomechanical loading. Despite the assumption that the emu wing is under minimal load, a moderate to high degree of laminarity was found in at least the humerus and ulna (Table 2). This laminarity can be attributed to the slow bone growth rate observed in the wing elements and/or to the third factor affecting bone microstructure: phylogenetic relationships. Within the paleognaths, it has been hypothesized that at least three independent flight losses have occurred, with only one order (the tinamous) still retaining the ability to fly (Harshman et al., 2008; Mitchell et al., 2014). The moderate/high wing bone laminarity may be a feature of the flighted common ancestor of paleognaths that is retained in the flightless descendants. Indeed, significant phylogenetic signal has been found in some osteohistological features in a sample of paleognaths (Legendre et al., 2014). Future studies should investigate the histological and *in vivo* loading of the flighted relatives of emus to better understand the potential influence of phylogeny on bone laminarity.

CONCLUSIONS

In the emu limb skeleton, ontogenetic factors such as adult size/age and slow growth rate are the dominant influence on vascular canal orientation. A weak but non-significant positive

438 correlation between laminarity and shear strain suggests that laminar bone is not a good predictor
 439 of torsional loading. Even though the forelimb elements likely experience minimal loading, the
 440 humerus and ulna exhibit variably moderate to high laminarity, perhaps due to phylogenetic
 441 encoding for this feature in avian forelimb bones or relatively slow growth rates, as have been
 442 observed with laminar bone in some other birds. Future studies should investigate laminarity in
 443 other palaeognathous birds to better understand the effects phylogeny, ontogeny, and torsional
 444 loading have on bone laminarity. Other future work should focus on the experimental
 445 manipulation of biomechanical loads to observe the effects on vascular canal orientation in limb
 446 bones and to better understand to what extent torsional load influences the development of limb
 447 bone laminarity. It is also important that variation found between different populations be
 448 addressed and studied further. Emu body mass growth rates vary among populations (e.g.
 449 Goonewardene et al., 2003), but it is unknown to what extent bone histology also varies with
 450 environmental, dietary, or genetic factors. This study has shown that in emu limb bones,
 451 laminarity reflects a complex interplay of ontogeny, biomechanical loads, and phylogeny.

453 ACKNOWLEDGEMENTS

454 The authors would like to thank K Ezell for assistance with histological preparation and imaging.
 455 We are grateful for free access to the microscopes in the Microscopy Core Facility at
 456 Midwestern University. We thank Dr. Andrew Biewener and the graduate students and postdocs
 457 at the Concord Field Station (2002-2006) for assistance with bone strain data collection. We
 458 thank reviewers Edina Prondvai and Jorge Cubo for useful comments that improved the
 459 manuscript.

460

461

REFERENCES

- Amprino R. 1947. La structure du tissu osseux envisagee comme expression de differences dans lavitesse de l'accroissement. *Archives de Biologie* 58:315–330.
- An YH, Martin KL. 2013. *Handbook of histology methods for bone and cartilage*. Humana Press; 1st edition.
- Biewener AA, Dial KP. 1995. In vivo strain in the humerus of pigeons (*Columba livia*). *Journal of Morphology* 225:61–75. DOI 10.1002/jmor.1052250106.
- Burnham KP, Anderson DR. 2002. *Model selection and multimodel inference: a practical information-theoretic approach*. New York: Springer-Verlag.
- Carrano MT, and Biewener AA. 1999. Experimental alteration of limb posture in the chicken (*Gallus gallus*) and its bearing on the use of birds as analogs for dinosaur locomotion. *Journal of Morphology* 240(3):237–249.
- Castanet J, Curry-Rogers K, Cubo J, Boisard JJ. 2000. Periosteal bone growth rates in extant ratites (ostriche [sic] and emu). Implications for assessing growth in dinosaurs. *Comptes Rendus de l'Academie des Sciences Serie III Sciences de la Vie* 323:543–550. DOI 10.1016/S0764-4469(00)00181-5.
- Cribari-Neto F, Zeileis A. 2010. Beta regression in R. *Journal of Statistical Software* 34:1-24.
- Curry JD. 2002. *Bones: Structure and Mechanics*. Princeton and University Press.
- de Ricqlès AJ, Meunier FJ, Castanet J, Francillon-Vieillot H. 1991. Comparative microstructure of bone. In: Hall BK, ed. *Bone, volume 3: bone matrix and bone specific products*. Boston: CRC Press, 1–78.
- de Margerie E. 2002. Laminar bone as an adaptation to torsional loads in flapping flight. *Journal of Anatomy* 201:521–526. DOI 10.1046/j.1469-7580.2002.00118.x.

485 de Margerie E, Cubo J, Castanet J. 2002. Bone typology and growth rates: testing and
486 quantifying ‘Amprino’s rule’ in the mallard (*Anas platyrhynchos*). *Comptes Rendus*
487 *Biologies* 325:221–230. DOI 10.1016/S1631-0691(02)01429-4.

488 de Margerie E, Robin JP, Verrier D, Cubo J, Groscolas R, Castanet J. 2004. Assessing a
489 relationship between bone microstructure and growth rate: a fluorescent labelling study in the
490 king penguin chick (*Aptenodytes patagonicus*). *Journal of Experimental Biology* 207:869–
491 879. DOI 10.1242/jeb.00841.

492 de Margerie E, Sanchez S, Cubo J, Castanet J. 2005. Torsional resistance as a principal
493 component of the structural design of long bones: comparative multivariate evidence in birds.
494 *Anatomical Record* 282A:49–66.

495 del Hoyo J, Elliot A, Sargatal J. eds. 1992. *Handbook of the Birds of the World*. Volume 1. Lynx
496 Edicions, Barcelona.

497 Ferrari S, Cribari-Neto F. 2004. Beta regression for modelling rates and proportions. *Journal of*
498 *Applied Statistics* 31(7):799–815. DOI: 10.1080/0266476042000214501.

499 Francillon-Vieillot H, de Buffrénil V, Castanet J, Géraudie J, Meunier FJ, Sire JY, Zylberberg L,
500 de Ricqlès A. 1990. Microstructure and mineralization of vertebrate skeletal tissues. In:
501 Carter JG, ed. *Skeletal Biomineralization: Patterns, Processes and Evolutionary Trends*.
502 *Volume 1*. New York: Van Nostrand Reinhold, 471–548.

503 Goonewardene LA, Wang Z, Okine E, Zuidhof MJ, Dunk E, Onderka D. 2003. Comparative
504 growth characteristics of Emus (*Dromaius novaehollandiae*). *The Journal of Applied Poultry*
505 *Research* 12(1):27–31.

506 Harshman, J, Braun EL, Braun MJ. 2008. Phylogenomic evidence for multiple losses of flight in
507 ratite birds. *Proceedings of the National Academy of Sciences of the United States of America*

508 105:13462–13467.

509 Hurvich CM, Tsai C-L. 1989. Regression and time series model selection in small samples.

510 *Biometrika* 76:297–307.

511 Lee AH, Simons ELR. 2015. Wing bone laminarity is not an adaptation for torsional loading in

512 bats. *PeerJ* 3:e823. DOI 10.7717/peerj.823.

513 Legendre LJ, Bourdon E, Scofield, RP, Tennyson A, Lamrous H, de Ricqlès AJ, Cubo J. 2014.

514 Bone histology, phylogeny, and palaeognathous birds (Aves: Palaeognathae). *Biological*

515 *Journal of the Linnean Society* 112:688–700.

516 Main RP, Biewener AA. 2007. Skeletal strain patterns and growth in the emu hindlimb during

517 ontogeny. *Journal of Experimental Biology* 20:2676–2690.

518 Marelli CA, Simons ELR. 2014. Microstructure and cross-sectional shape of limb bones in Great

519 Horned Owls and Red-tailed Hawks: how do these features relate to differences in flight and

520 hunting behavior? *PloS one* 9(8):e106094.

521 Maxwell EE, Larsson HCE. 2007. Osteology and myology of the wing of the emu (*Dromaius*

522 *novaehollandiae*), and its bearing on the evolution of vestigial structures. *Journal of*

523 *Morphology* 268:423–441. DOI: 10.1002/jmor.10527.

524 Mitchell KJ, Llamas B, Soubrier J, Rawlence NJ, Worthy TH, Wood J, Cooper A. 2014. Ancient

525 DNA reveals elephant birds and kiwi are sister taxa and clarifies ratite bird evolution.

526 *Science* 344(6186):898–900

527 Montes L, de Margerie E, Castanet J, de Ricqlès AJ, Cubo J. 2005. Relationship between bone

528 growth rate and the thickness of calcified cartilage in the long bones of the Galloanserae

529 (Aves). *Journal of Anatomy* 206:445–452.

530 Ourfalian RM, Ezell K, Lee AH. 2016. Development of wing bone laminarity in the pigeon. *The*

531 *Official Journal of the Federation of American Societies for Experimental Biology*
532 30:779.12.

533 Padian K. 2013. Why study the bone microstructure of fossil tetrapods? In: Padian K, Lamm E-
534 T, eds. *Bone Histology of Fossil Tetrapods: Advancing Methods, Analysis, and*
535 *Interpretation*. California: University of California Press, 1–11.

536 Pratt IV, Cooper DML. 2017. A method for measuring the three-dimensional orientation of
537 cortical canals with implications for comparative analysis of bone microstructure in
538 vertebrates. *Micron* 92:32–38.

539 Pratt IV, Cooper DML. 2018. The effect of growth rate on the three-dimensional orientation of
540 vascular canals in the cortical bone of broiler chickens. *Journal of Anatomy* 233:531–541.

541 Pratt IV, Johnston JD, Walker E, Cooper DML. 2018. Interpreting the three-dimensional
542 orientation of vascular canals and cross-sectional geometry of cortical bone in birds and bats.
543 *Journal of Anatomy* 232(6):931–942.

544 R Development Team. 2018. *R: A language and environment for statistical computing*. Vienna,
545 Austria: R Foundation for Statistical Computing.

546 Riggs CM, Lanyon LE, Boyde A. 1993. Functional associations between collagen fibre
547 orientation and locomotor strain direction in cortical bone of the equine radius. *Anatomy and*
548 *Embryology* 187:231–238.

549 Rubin CT, Lanyon LE. 1985. Regulation of bone mass by mechanical strain magnitude.
550 *Calcified tissue international* 37(4):411–417.

551 Simons ELR, O'Connor PM. 2012. Bone laminarity in the avian forelimb skeleton and its
552 relationship to flight mode: testing functional interpretations. *The Anatomical Record*
553 295:386–396. DOI 10.1002/ar.22402.

554 Skedros JG, Hunt KJ. 2004. Does the degree of laminarity correlate with site-specific differences
555 in collagen fibre orientation in primary bone? An evaluation in the turkey ulna diaphysis.
556 *Journal of Anatomy* 205:121–134.

557 Skedros JG, Hunt KJ, Bloebaum RD. 2004. Relationships of loading history and structural and
558 material characteristics of bone: development of the mule deer calcaneus. *Journal of*
559 *Morphology* 259(3):281–307.

560 Skedros JG, Doutré MS. 2019. Collagen fiber orientation pattern, osteon morphology and
561 distribution, and presence of laminar histology do not distinguish torsion from bending in at
562 and pigeon bones. *Journal of Anatomy Early View*. doi.org/10.1111/joa.12981

563 Smithson M, Verkuilen J. 2006. A better lemon squeezer? Maximum-likelihood regression with
564 beta-distributed dependent variables. *Psychological Methods* 11:54–71. DOI: 10.1037/1082-
565 989X.11.1.54.

566 Swartz SM, Bennett MB, Carrier DR. 1992. Wing bone stresses in free flying bats and the
567 evolution of skeletal design for flight. *Nature* 359:726–729.

568 Taper ML. 2004. Model identification from many candidates. In: Taper ML, Lele SR eds. *The*
569 *Nature of Scientific Evidence: Statistical, Philosophical, and Empirical Considerations*.
570 Chicago, Illinois: University of Chicago Press, 488–524.

571 van Gaalen SM, Kruyt M, Geuze RE, de Bruijn JD, Alblas J, Dhert WJ. 2010. Use of
572 fluorochrome labels in in vivo bone tissue engineering research. *Tissue Engineering Part B:*
573 *Reviews* 16: 209–217.

574 Warton DI, Hui FKC. 2011. The arcsine is asinine: the analysis of proportions in ecology.
575 *Ecology* 92(1):3–10.

576 Williams B, Waddington D, Murray DH, Farquharson C. 2004. Bone strength during growth:

577 influence of growth rate on cortical porosity and mineralization. *Calcified Tissue*
 578 *International* 74:236–245.
 579

Figure 1

Representative histological sections of emu femora, tibiotarsi, and humeri from a range of ages.

2.3 weeks (A, B, C), 8.1 weeks (D, E), 12 weeks (F), 16 weeks (G, H, I), 60 weeks (L, J, K).

Femora (A, D, G, J), tibiotarsus (B, E, H, K) and humeri (C, F, I, L). Scale bars equal 1000 μ m for femora and tibiotarsi, and 250 μ m for humeri. Bright field images of non-straightened caudal or medial octants (10x magnification).

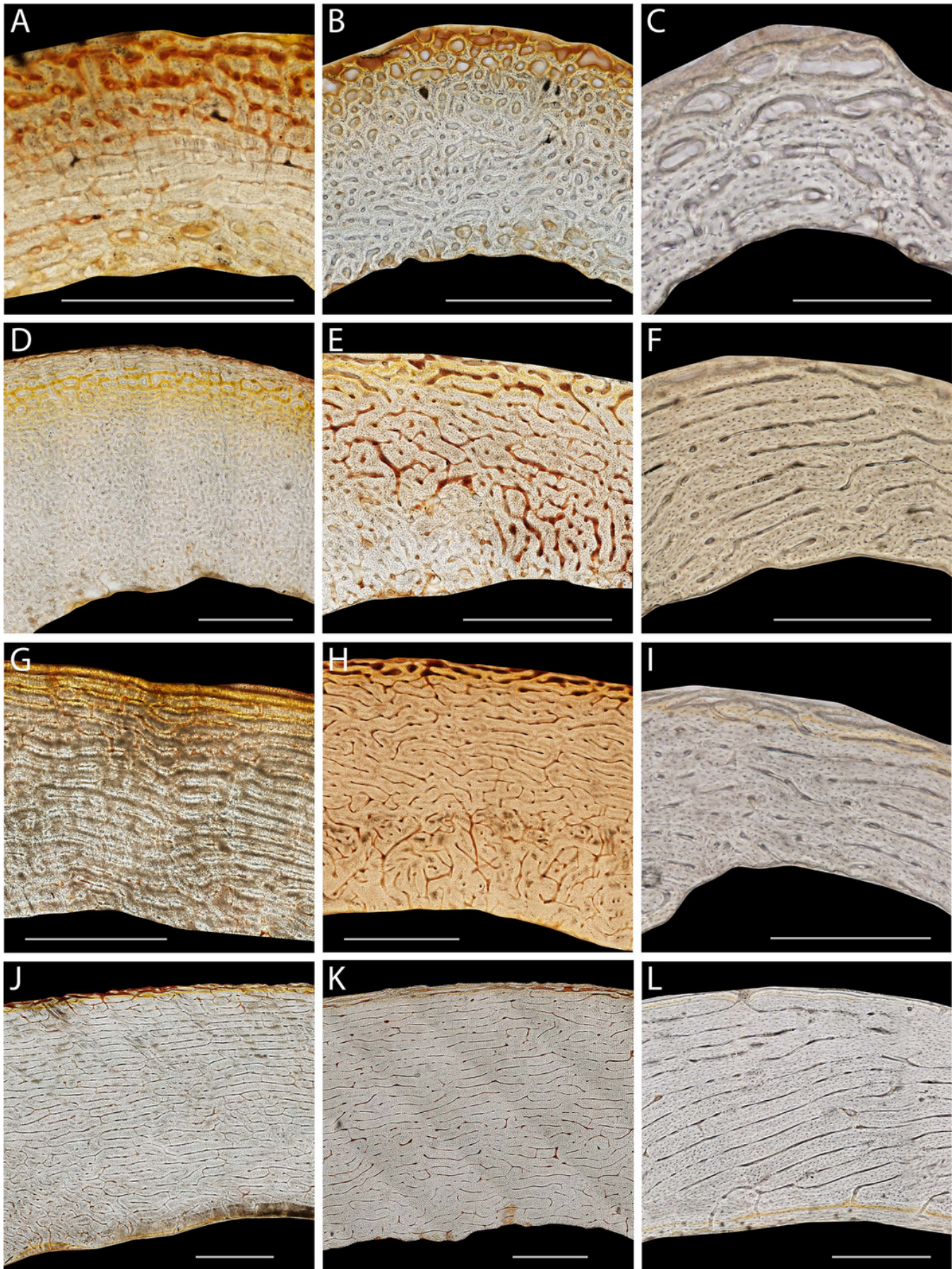


Figure 2

Sampling methods for growth rate and laminarity measures.

(A) Gray shading indicates the four octants (wing elements: cranial, caudal, dorsal, ventral; hindlimb elements: cranial, caudal, lateral, medial) sampled on each cross-section. (B) Each octant was isolated, straightened, and a sample area indicated: between fluorochrome reference lines. (C) On fluorescent images, growth rate was measured by taking the mean distance (white arrow) between the periosteal extent of the xylenol (appears red) and calcein (green/yellow) tags divided by number of days between injections. (D) Laminarity was measured by drawing an ellipse in each in-focus primary vascular canal and determining the proportion of circumferential canals. (Tibiotarsus 17, 4.6 wks).

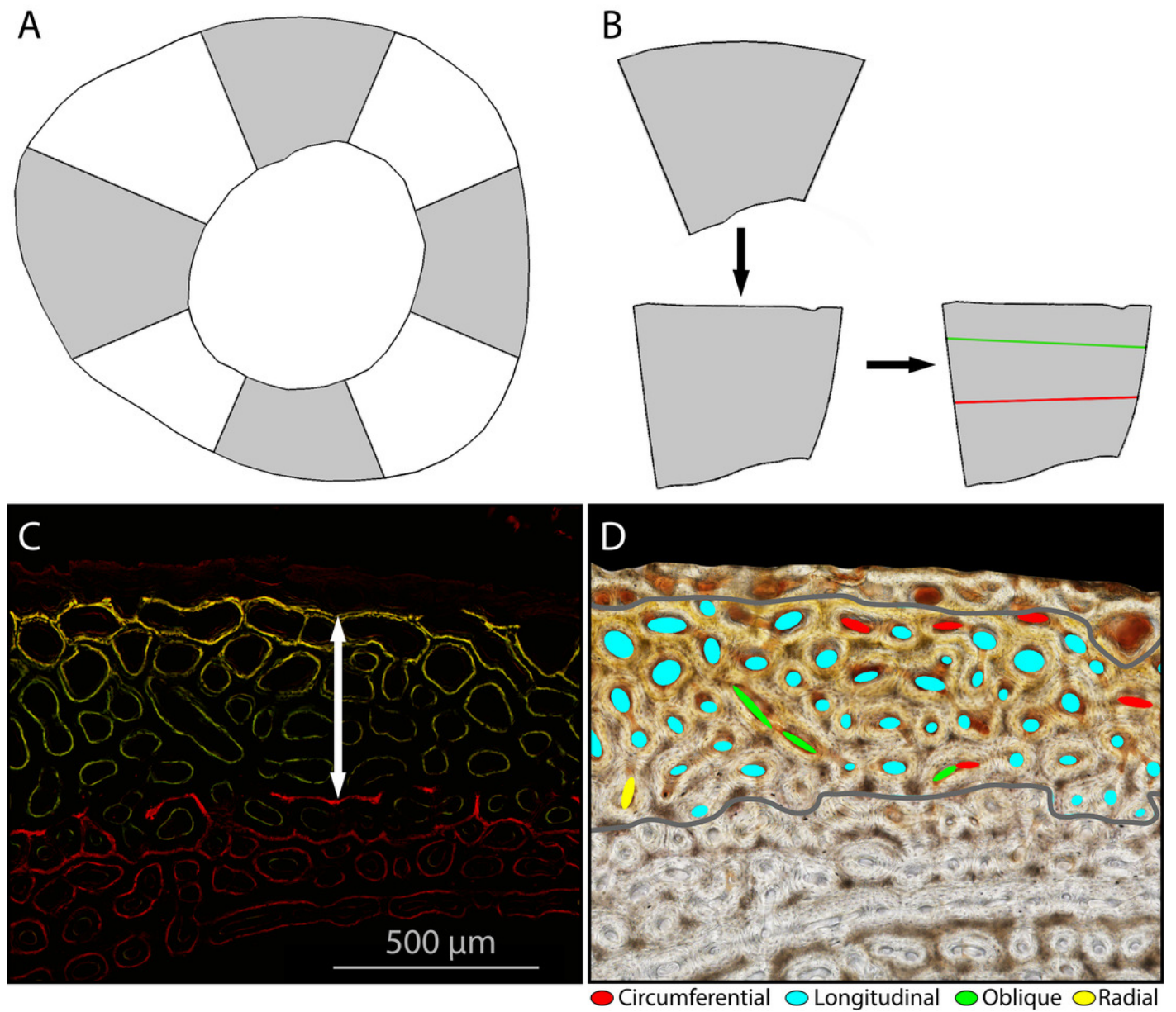


Figure 3

Laminarity Indices for the forelimb and hindlimb bones included in this study.

Laminarity indices (LI) measured for each bone (Fem=femur, Tbt= tibiotarsus, Hum=humerus, Ulna, Rad=radius) from specimens (A) 15 - 2 week, (B) 1c - 2 week, (C) 17 - 5 week, (D) 14b - 8 week, (E) 16 - 12 week, (F) 2a - 16 week, (G) 21 - 48 week, and (H) 23 - 60 week. LI was measured between fluorochrome reference lines on all sampled octants.

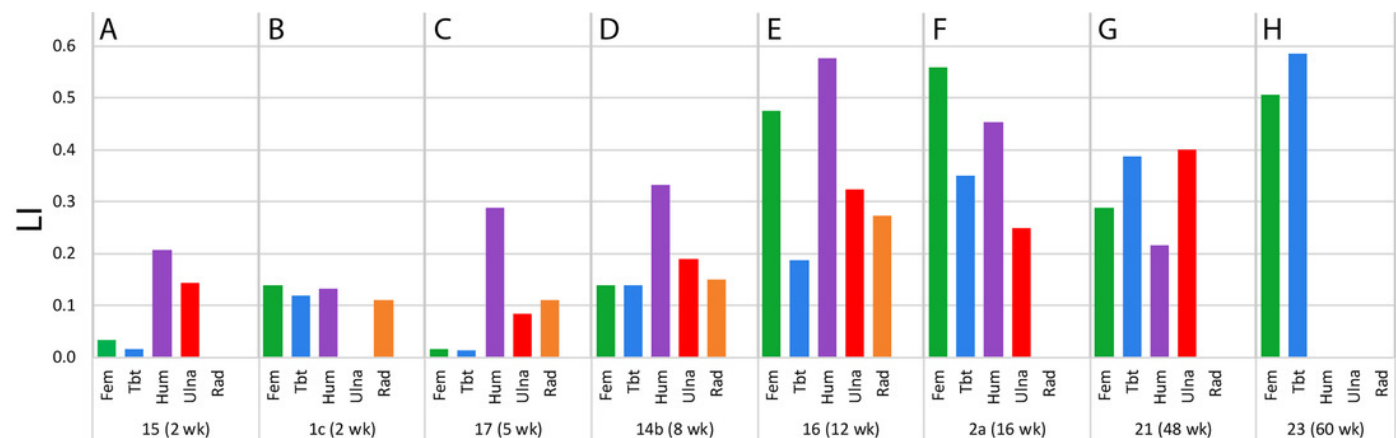


Figure 4

Principal components analysis of the caudal octants from the femur and tibiotarsus.

An “ontogenetic axis” (PC 1) accounts for 75% of the variance with juvenile features to the left (small size, young age, and rapid growth) and adult features to the right (large size, old age, and slow growth). An orthogonal “shear strain axis” (PC 2) explains another 20% of the cumulative variance.

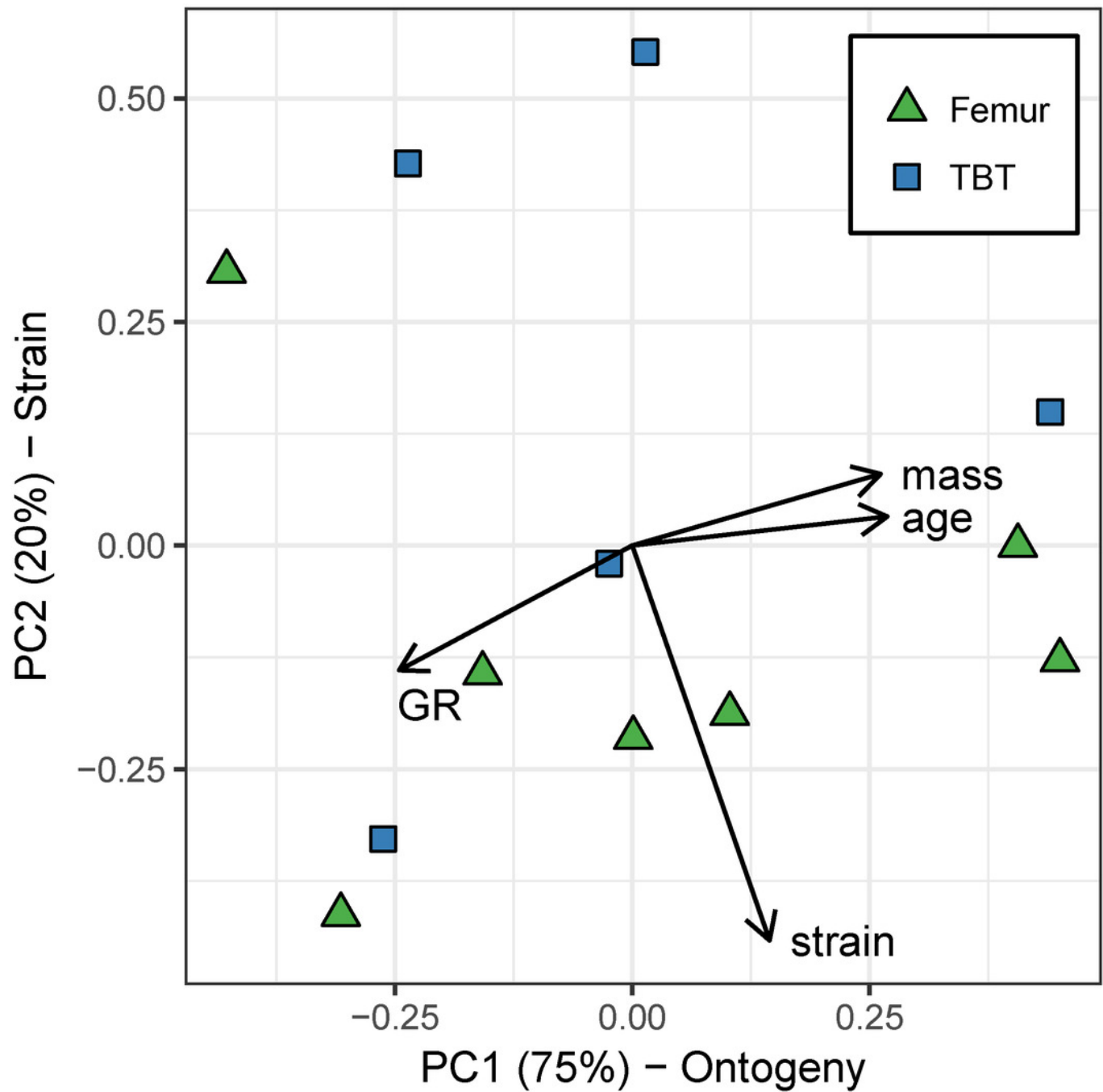

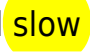


Figure 5

Caudal octant laminarity (LI) in the hindlimb depends primarily on the “ontogenetic axis” and secondarily on the “shear strain axis”.

Beta regression was performed on data from the femur (green triangles) and tibiotarsus (blue squares). The “ontogenetic axis” accounts for 43% of the variation in caudal octant laminarity, whereas the “shear strain axis” explains 18% of the variation. (A) When the effect of shear strain is controlled, there is a significant positive correlation between laminarity and the ontogenetic axis ($p = 0.002$). (B) However, when the effect of ontogeny is controlled, laminarity and the shear strain axis show a weak positive association ($p = 0.052$). These results generally suggest the laminarity of newly formed periosteal bone in the caudal octant of the femur and tibiotarsus is largely dependent on ontogenetic factors. Elevated  laminarity values are strongly correlated with adult features such as large size, old age, and  slow growth rate.

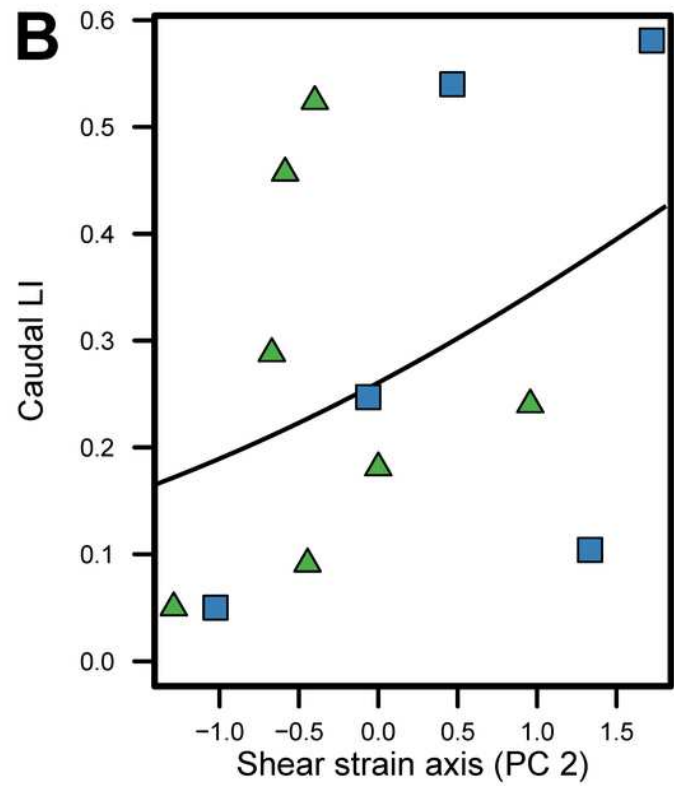
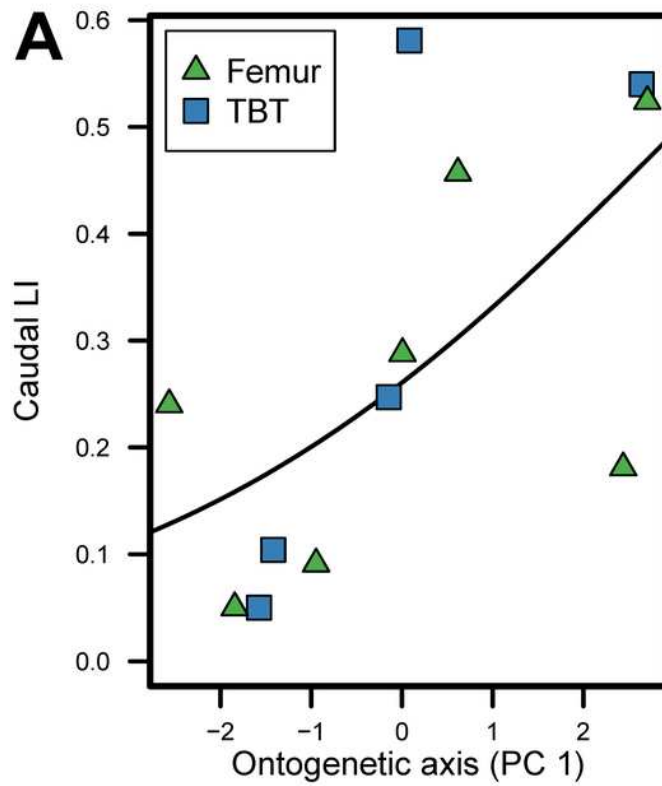


Figure 6

Principal components analysis of the four cardinal octants from the femur and tibiotarsus.

An “ontogenetic axis” (PC 1) accounts for 94% of the variance with juvenile features to the left (small size, young age, and rapid growth) and adult features to the right (large size, old age, and slow growth). Residual variation from growth rate largely contributes to an “ontogeny-independent growth rate axis” along PC 2. This axis only explains 5% of the cumulative variance.

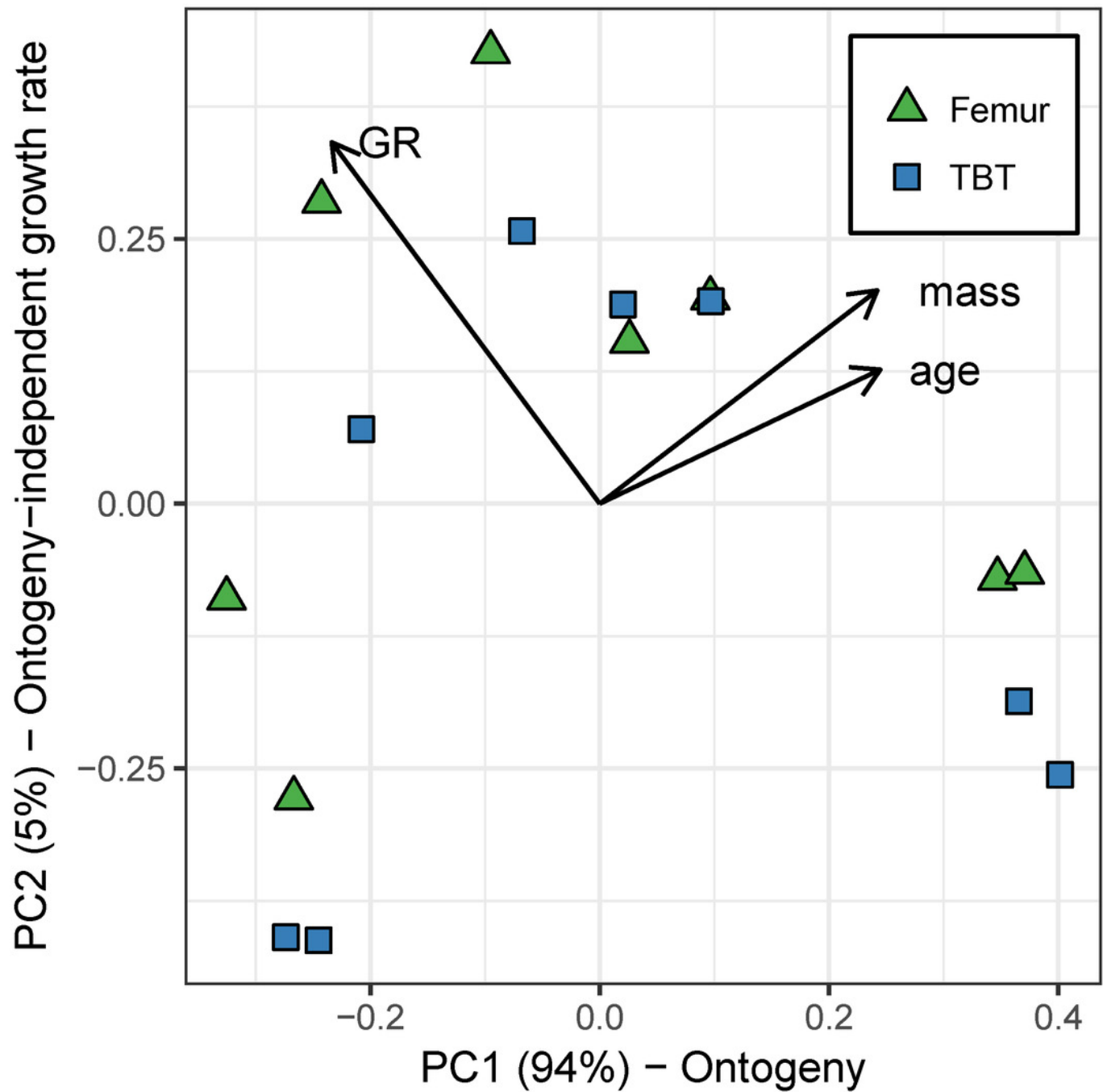



Figure 7

The “ontogenetic axis” has a strong influence on mean laminarity (LI) in the hindlimb.

Analysis was performed using beta regression with element [femur (green triangles) and tibiotarsus (blue squares)] as an additive cofactor. Juvenile features (e.g., small size, young age, and rapid growth rate) are correlated with lower laminarity values, whereas adult features are correlated with high laminarity values ($p < 0.001$). The “ontogenetic axis” explains 70% of the variation in laminarity across cardinal octants in the femur and tibiotarsus.  When the effect of ontogeny is controlled, laminarity is slightly higher in the femur than in the tibiotarsus. However, this difference is minor and only accounts for 2% of the variation in laminarity.

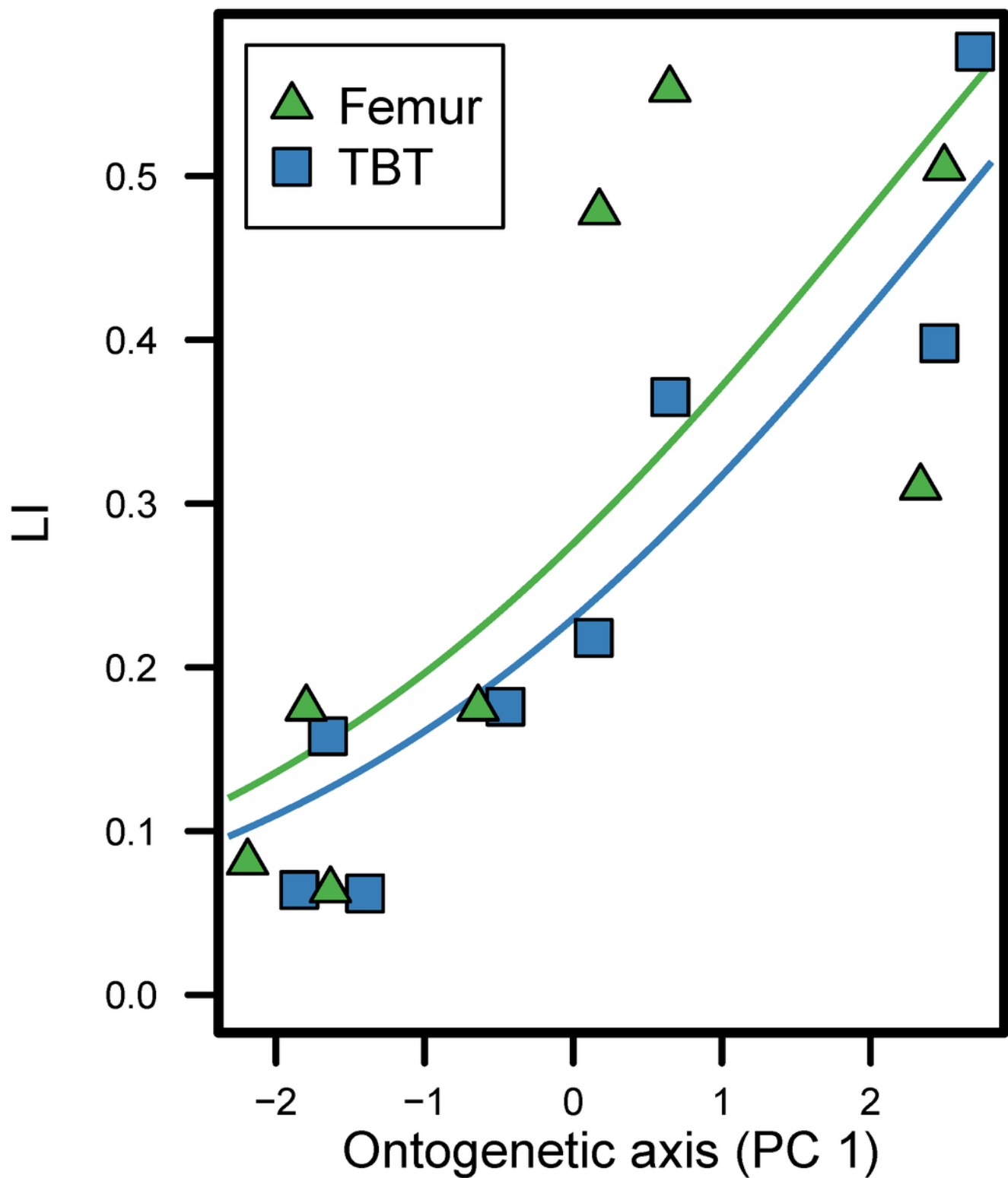


Figure 8

Principal components analysis of the four cardinal octants from the humerus, ulna, and radius.

An “ontogenetic axis” (PC 1) accounts for 87% of the variance with juvenile features to the left (small size, young age, and rapid growth) and adult features to the right (large size, old age, and slow growth). Residual variation from growth rate largely contributes to an “ontogeny-independent growth rate axis” along PC 2. This axis explains 12.6% of the cumulative variance.

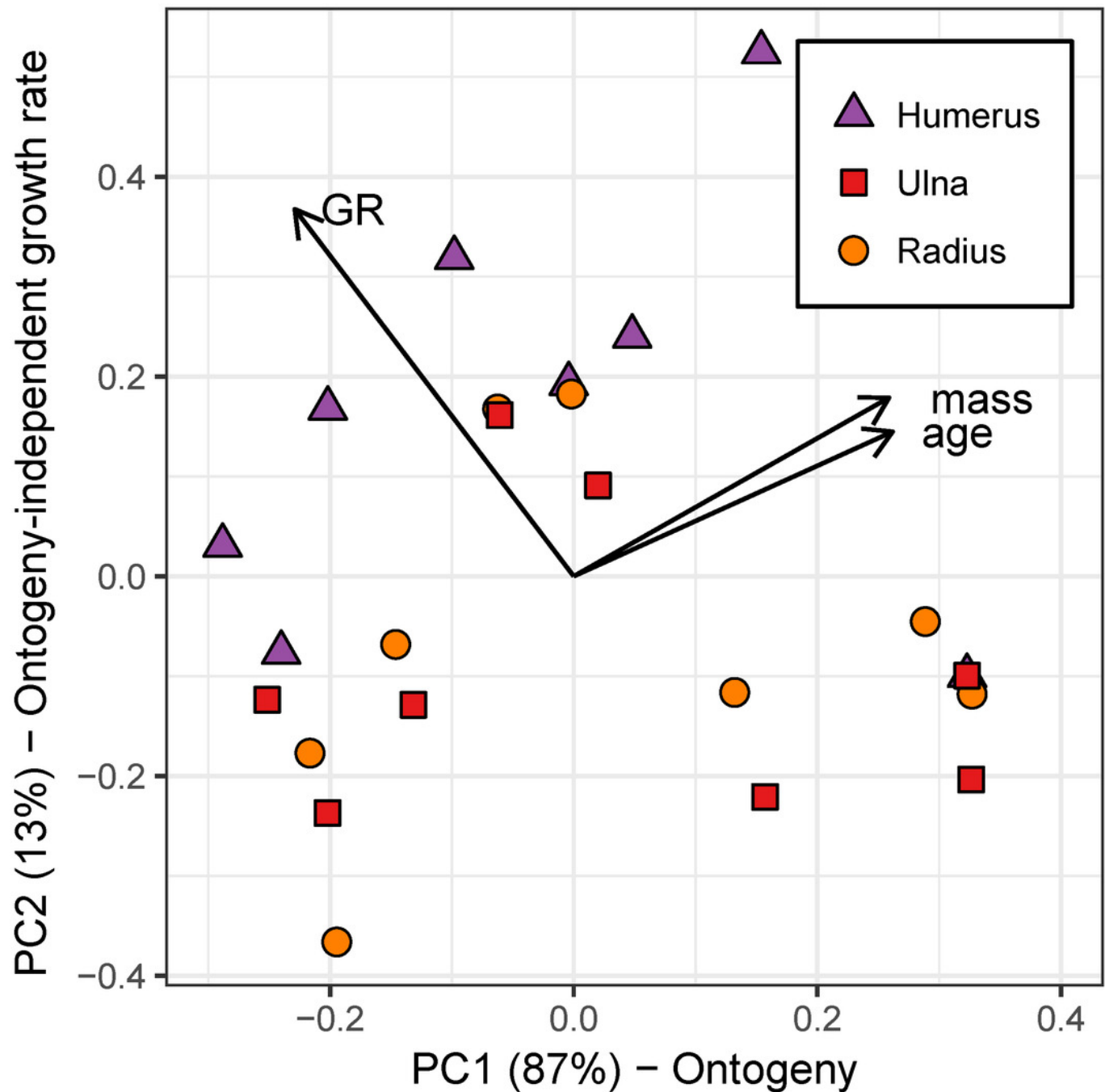


Figure 9

Mean laminarity (LI) in forelimb elements depends on “ontogeny-independent growth rate.”

Beta regression was performed on data from the humerus (purple triangles), ulna (red squares), and radius (orange circles). One of the best supported models suggests that laminarity depends in part on the “ontogenetic axis” and residual variation in growth rate (“ontogeny-independent growth rate”) as additive covariates. (A) The effect of “ontogenetic axis” is small and accounts for 4–5% of the variation in laminarity. Ontogeny and laminarity in the forelimb elements are poorly correlated ($p = 0.287$). (B) However, the effect of “ontogeny-independent growth rate” is stronger and explains 39% of the variation in laminarity. In addition, a positive correlation is supported ($p = 8.77e-5$).

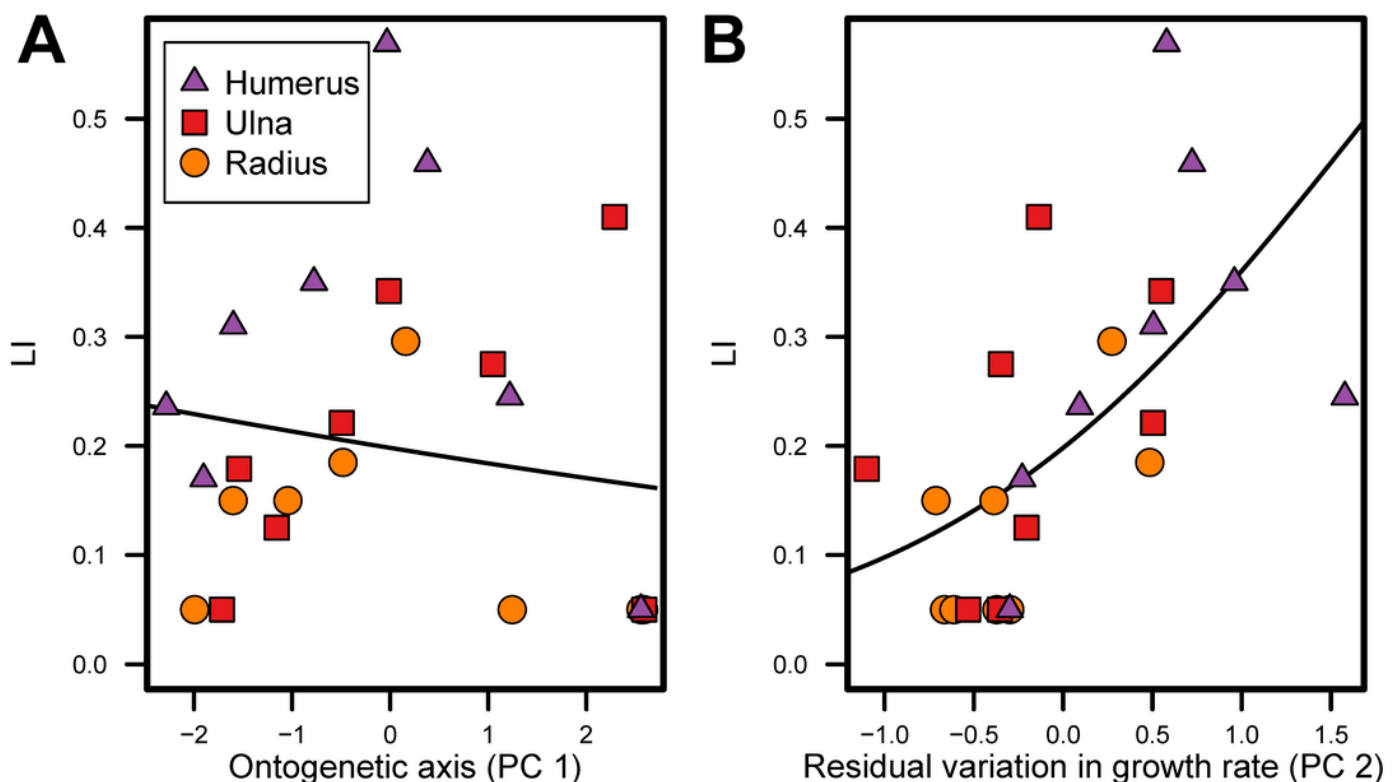


Table 1 (on next page)

Emu identification number, age at sacrifice, and mass.

1

Specimen	Age (weeks)	Mass (kg)
15	2.3	0.74
1c	2.4	0.94
17	4.6	1.53
14b	8.1	4.73
16	12	6.85
2a	15.9	11.13
21	48	28.9
23	60.1	29.4

2

3

4

Table 2(on next page)

Growth rate and bone laminarity for emu specimens.

Laminarity Index (LI) was measured in a sample area outlined by the periosteal extent of two bone fluorochromes.

Specimen	Age (weeks)	Element	Growth Rate (um/day)	LI
15	2.3	Femur	130.16	0.03
		Tibiotarsus	62.31	0.02
		Humerus	25.44	0.21
		Ulna	6.75	0.14
		Radius	15.22	0
1c	2.4	Femur	73.3	0.14
		Tibiotarsus	53.82	0.12
		Humerus	16.22	0.13
		Ulna	11.57	0
		Radius	9.49	0.11
17	4.6	Femur	162.62	0.02
		Tibiotarsus	99.11	0.01
		Humerus	25.15	0.29
		Ulna	11.54	0.08
		Radius	9.36	0.11
14b	8.1	Femur	101.14	0.14
		Tibiotarsus	68.46	0.14
		Humerus	23.83	0.33
		Ulna	14.4	0.19
		Radius	14.14	0.15
16	12	Femur	38.25	0.48
		Tibiotarsus	41.48	0.19
		Humerus	12.17	0.58
		Ulna	11.77	0.32
		Radius	8.65	0.27
2a	15.9	Femur	29.42	0.56
		Tibiotarsus	29.2	0.35
		Humerus	11.07	0.45
		Ulna	3.36	0.25
		Radius	2.37	0
21	48	Femur	6.43	0.29
		Tibiotarsus	4.94	0.39
		Humerus	14.55	0.22
		Ulna	2.18	0.40
		Radius	1.33	0
23	60.1	Femur	5.9	0.51

		Tibiotarsus	3.8	0.58
		Humerus	1.7	0
		Ulna	1.62	0
		Radius	1.67	0

1

Table 3(on next page)

Caudal shear strain and caudal octant laminarity for emu specimens.

Shear strain data was previously collected by Main and Biewener (2007). Laminarity Index (LI) was measured in a sample area outlined by the periosteal extent of two bone fluorochromes in the caudal octant only. n/a indicates elements for which there was no strain data.

1

Specimen	Age (weeks)	Element	Caudal Shear Strain (microstrain)	Caudal Octant LI
15	2.3	Femur	n/a	0
		Tibiotarsus	n/a	0
1c	2.4	Femur	-308	0.21
		Tibiotarsus	n/a	0.13
17	4.6	Femur	-1503	0
		Tibiotarsus	-1397	0
14b	8.1	Femur	-997	0.05
		Tibiotarsus	-261	0.06
16	12	Femur	-1491	0.26
		Tibiotarsus	-947	0.22
2a	15.9	Femur	-1620	0.45
		Tibiotarsus	-293	0.59
21	48	Femur	-1657	0.15
		Tibiotarsus	-1318	0.55
23	60.1	Femur	-2283	0.53
		Tibiotarsus	n/a	0.81

2

3

Table 4(on next page)

Summary of principal components analyses.

Caudal Octants from Femur and Tibiotarsus				
	PC 1	PC 2	PC 3	PC 4
Eigenvalues	3.001	0.812	0.180	0.008
Standard deviation	1.732	0.901	0.424	0.087
Proportion of variation	0.750	0.203	0.045	0.002
Cumulative Proportion	0.750	0.953	0.998	1.000
Mass	0.555	0.170	0.515	0.63
Age	0.570	—	0.296	-0.763
Shear strain	0.307	-0.937	-0.135	—
Growth rate	-0.521	-0.296	0.793	-0.109
Cardinal Octants from Femur and Tibiotarsus				
	PC 1	PC 2	PC 3	
Eigenvalues	2.835	0.157	0.009	
Standard deviation	1.684	0.396	0.093	
Proportion of variation	0.945	0.052	0.003	
Cumulative Proportion	0.945	0.997	1.000	
Mass	0.582	0.484	0.654	
Age	0.588	0.304	-0.749	
Growth rate	-0.562	0.820	-0.108	
Cardinal Octants from Humerus, Ulna, and Radius				
	PC 1	PC 2	PC 3	
Eigenvalues	2.614	0.377	0.010	
Standard deviation	1.617	0.614	0.099	
Proportion of variation	0.871	0.126	0.003	
Cumulative Proportion	0.871	0.997	1.000	
Mass	0.597	0.412	0.688	
Age	0.604	0.334	-0.721	
Growth rate	-0.528	0.848	—	

1

Table 5(on next page)

Comparison of beta regression models.

Best supported models have the smallest Akaike's Information Criterion (AIC_c) value and ΔAIC_c less than 3. Principal components (PC) with significant coefficient values are marked with asterisks (*).

Caudal Octants from Femur and Tibiotarsus									
Model: LI ~	Pseudo-R ²	AIC _c	ΔAIC _c	PC 1	PC 2	Fem PC 1	TBT PC 1	Fem PC 2	TBT PC 2
PC 1	0.426	-6.9	0.0	0.341*					
PC 2	0.184	-2.6	4.3		0.372				
PC 1 + PC 2	0.610	-5.5	1.4	0.340*	0.411				
element + PC 1	0.429	-2.6	4.3	0.355*					
element + PC 2	0.208	1.9	8.8		0.417				
element + PC 1 + PC 2	0.623	0.7	7.6	0.337*	0.450				
element × PC 1	0.501	2.4	9.3			0.260	0.270		
element × PC 2	0.219	8.1	14.9					0.285	0.219
element × PC 1 + element × PC 2	0.660	21.0	27.9			0.252*	0.267	0.324	0.221
Cardinal Octants from Femur and Tibiotarsus									
Model: LI ~	Pseudo-R ²	AIC _c	ΔAIC _c	PC 1	PC 2	Fem PC 1	TBT PC 1	Fem PC 2	TBT PC 2
PC 1	0.703	-24.4	0.0	0.438*					
PC 2	0.001	-6.4	18.0		0.067				
PC 1 + PC 2	0.703	-21.1	3.4	0.448*	0.192				
element + PC 1	0.723	-21.7	2.8	0.442*					
element + PC 2	0.011	-17.7	6.7		0.014				
element + PC 1 + PC 2	0.721	-17.4	7.1	0.447*	0.108				
element × PC 1	0.726	-17.2	7.3			0.399*	0.095		
element × PC 2	0.013	1.4	25.9					-0.09	0.184
element × PC 1 + element × PC 2	0.724	-5.8	18.6			0.409*	0.086	0.194	-0.16
Cardinal Octants from Humerus, Ulna, and Radius									
Model: LI ~	Pseudo-R ²	AIC _c	ΔAIC _c	PC 1	PC 2	Hum PC 1	Ulna PC 1	Rad PC 1	Hum PC 2
PC 1	0.048	-26.2	10.6	-0.084					
PC 2	0.389	-36.8	0.0		0.828*				
PC 1 + PC 2	0.435	-35.1	1.6	-0.092	0.824*				
element + PC 1	0.259	-25.8	11.0	-0.065					
element + PC 2	0.443	-32.4	4.3		0.719*				
element + PC 1 + PC 2	0.482	-29.9	6.9	-0.082	0.728*				
element × PC 1	0.317	-19.6	17.2			-0.137	0.219	0.013	
element × PC 2	0.449	-25.1	11.7						0.628
element × PC 1 + element × PC 2	0.532	-12.2	24.6			-0.187	0.261	0.085	0.715*

Cardinal Octants from Humerus, Ulna, and Radius									
Model: LI ~	Ulna PC 2	Rad PC 2							
PC 1									
PC 2									
PC 1 + PC 2									
element + PC 1									
element + PC 2									
element + PC 1 + PC 2									
element × PC 1									
element × PC 2	0.101	0.399							
element × PC 1 + element × PC 2	0.036	0.251							

2